The Proposition of a Dual-Sensitivity Laminated Multimetal Dielectric Stacks Detecting Structure Based on the Reflected Goos–Hänchen Effect

Yuan-Kun Shi, You-Ming Liu, and Hai-Feng Zhang

***Abstract*—Future advancements in integration technologies will significantly benefit from the creation and innovation of passive nonreciprocal detecting devices. The present work proposes a novel passive multiwaveguide stacking (MWS) detecting structure, which enjoys a prominent passive nonreciprocal property. By introducing envelope contents asymmetrically, the resonant modes of the forward and backward incident electromagnetic waves (EWs) could be differentiated in the near-infrared band, accompanied by an enhanced reflected Goos–Hänchen (GH) effect. Because of the asymmetry of the laminar structure and the metal layers, the local address of the photon energy at the resonance of the forward and backward incidence could be significantly misaligned, along with distinct sensitivities toward the alternation of the designated layer under passive conditions. Furthermore, to satisfy the demands of a growing area of sensing through the transfer matrix method and the stationary phase method, the performance of the detector in terms of refractive index (RI) is also discussed. This work aims to enlighten the design of a nonreciprocal GH detecting device for multiple physical scenarios under nonreciprocal effect and provide some fresh concepts for creating new passive integrated devices.**

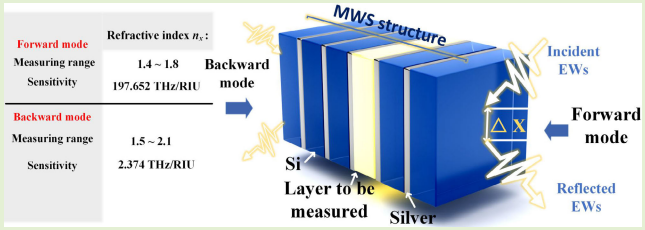

***Index Terms*— 1-D photonic waveguide structure, Goos–Hänchen (GH) effect, nonreciprocal feature, stationary phase method, transfer matrix method.**

I. Introduction

RECENTLY, the focus has been tightly attached to the Goos–Hänchen (GH) shift for the profound application potential, which typically describes a lateral shift (LS) arising involving points of light emission and incidence at the surface of a collimated beam [1], [2]. Commonly, because a real incident beam comprises several plane waves with faintly different incident angles and because the reflection phase varies with the incident angle, when plane waves are mirrored and reconverge into a reflected beam, a miniature transverse spatial shift will be produced in the macroscope. Additionally, GH angle shift will occur when the interface has different reflection coefficients for the decomposed plane waves [3], [4].

Howbeit, the spatial GH effects generated from customary total internal reflection systems are universally exhibited at the wavelength magnitude, necessitating a customary resort to the weak measurement [5], which imposes a terrific limitation on the integration of the GH device. Hence, enhancing the GH effect manifests desperate importance, particularly in terms of application areas.

Scholars have made a myriad of constructive endeavors to the enhancement of the GH effect. If divided by material type, the central attempts could be divided into magneto-optic materials [6], electro-optic materials [7], metamaterials [8], [9], [10], double-negative materials [11], [12], [13], graphene [14], [15], and so on. If divided by the structure, it could be summarized as frustrated total internal reflection implement [16], absorbent medium plate [17], [18], attenuated total reflection structure [19], parity-time symmetric interfaces [20], surface plasmon resonance (SPR) structures [21], [22], [23], photonic crystals [24], [25], optical waveguide [26], [27], [28], and so on. Besides, through a purposeful combination of materials and structures based on diverse physical backgrounds, the laminated photonics structures are worth elaborating on, which show unrelenting heat due to the unique physical state of the interface resulting from the particular photonic localization of

Manuscript received 15 October 2023; revised 3 December 2023; accepted 4 December 2023. Date of publication 12 December 2023; date of current version 12 January 2024. This work was supported by the College Student Innovation Training Program of Nanjing University of Posts and Telecommunications. The associate editor coordinating the review of this article and approving it for publication was Dr. Anuj Kumar Sharma. *(Yuan-Kun Shi and You-Ming Liu contributed equally to this work.) (Corresponding author: Hai-Feng Zhang.)*

The authors are with the College of Electronic and Optical Engineering and the College of Flexible Electronics (Future Technology), Nanjing University of Posts and Telecommunications, Nanjing 210023, China (e-mail: hanlor@163.com).

This article has supplementary downloadable material available at https://doi.org/10.1109/JSEN.2023.3340171, provided by the authors.

Digital Object Identifier 10.1109/JSEN.2023.3340171

the system. It has also brought numerous unique perspectives to advancing the GH effect. Typically, the reflected phase bias produced by the band edge state [29] or the defect mode [24] is subtle. In recent years, Singh's team discovered near the Brewster angle a lossy layer in the stack brings out the singular phase and enhances GH shift at the point of darkness [30], [31]. The effect can be utilized to detect the glycerol solution and hydrogen gas [32], [33]. However, the generation of GH shift is not necessarily limited to oblique incidence; it can also occur under normal incidence, which can be attributed to the interference between the leaky guided modes of the coupled chains [34]. Scholars discovered another novel physical phenomenon produced on periodic dielectric layers that could enhance the GH effect—Bloch surface wave, which manifests at the interface of a truncated stack of periodically alternating dielectric layers [35], and this novel physical phenomenon demonstrates to be a successful strategy for boosting the GH phenomenon. Furthermore, researchers have also discovered interfacial states that do not require excitation by external extra structures through conjugated photonic crystals with different topological states [36], [37], as well as optical Tamm states generated by 1-D photonic crystals bonded to metal layers [38]. By realizing the quasibound states in the continuum with ultrahigh Q factors, the GH shift can be greatly enhanced to the orders of wavelength [39]. Last but not least, there are interesting phenomena between the GH shift and the polarization of light. In the chiral quantum-dot molecule system, the GH shifts of transmitted and reflected beams are greatly affected by right-handed circularly polarized and left-handed circularly polarized light, and the GH shifts of right-handed circularly polarized light are enhanced [40].

Along with the theoretical enhancement research based on laminated photonics structures, the design of the laminated GH-detecting structure has also currently witnessed a significant evolution in the application domain. Additionally, Kong et al. [41] devised and experimentally verified a very responsive refractive index (RI) detector predicated on the Bloch surface wave induction scheme. The system is relatively compact, which displays great application potential for the GH sensing structure. In addition, theoretically, a bimetallic detector founded on hexagonal boron nitride heterostructure and graphene is investigated by Liu et al. [42], and the sensitivity turns out to be 2.02×10^5 λ/RI unit (RIU). It deserves attention that the tweaking of the Fermi energy level of the graphene also led to the development of tunable sensitivity, which is a crucial aspect of sensor design. Despite being customizable, the sensitivity sustains a limited range and does not discriminate effectively between various physical modes.

The waveguide structure is another domain of the enhancement of the GH effect. When the incident light beam meets a specified guiding mode criterion, the light field energy will be stabilized within a dielectric layer with the given dielectric thickness, giving birth to a giant LS onto the surface. Due to the strong localization of the optical field, the detection of substance to be measured under this localized mode enjoys a high sensitivity, thus giving rise to a series of research works for detection. Previous generations have created several deftly planned and high-performance sensing devices. Yu et al. [43] suggested an oscillating wave displacement detector based on the improved GH effect in an optical waveguide with symmetrical metal cladding. The results show an excellent sensitivity of 1.6 pm in theory and practically produce a displacement resolution of 40 pm with a straightforward and easily fabricable framework. Wang et al. [44] proposed a symmetrical metal-cladding waveguide (SMCW) detecting structure. On the thermal optic and thermal expansion effects, the SMCW structure displays a great resolution of approximately 5×10^{-3} °C, the excitation of the ultrahigh-order mode generates an enhanced GH shift, which is meaningful for the actual application. Moreover, Hedhly et al. [45] put forward a plasmonic waveguide biosensor. It is a symmetric metal cladding plasmonic waveguide structure, and the presentation turned out to be meaningful for the proposal is a further development of the traditional waveguide structure enabling the structure to detect small molecules, such as glycerol and M biotin.

Whether based on waveguide structures or layered photonic structures, it is easy to establish that the most common sensor design is based on detecting a single physical quantity. Suppose we want to implement the detection of several physical quantities, one of the shortcuts is to attain a solid nonreciprocal feature, which is an intriguing area for further research. Even though mountains of the GH effect-based devices mentioned above have achieved excellent sensing talents in various application scenarios, it is imperative to recognize that although they majorly succeed in one detection window or one type of measurement precision, the development of today's sensors necessitates more and more multifunctional or multiphysical scenario devices, which bring the potential of lower cost and further improvements in the device integration.

Considering the enormous current gap in GH device design for multiphysics settings, a multiwaveguide stacking (MWS) detecting structure containing asymmetric topological defects along with metal layers is theoretically designed. It is an innovative combination of a laminar photonic structure and a metallic waveguide structure. It combines the high sensitivity of conventional waveguide structures with the unique characteristics of multilayer photonics crystal stacking structures. After optimization and adjustment, it is found that the novel proposal enjoys the ability to implement nonreciprocal high-sensitivity sensors passively. As a result of the significantly disparate resonance mode of the microcavity, the forward and backward sensing patterns of the given GH device establish distinct detecting talents under the passive condition, respectively, which is the fundamental merit of the structure. For the forward incidence and negative incidence, the designed MWS can detect the refractive indexes between 1.4 and 1.8 RIU and 1.5 and 2.2 RIU, respectively. In nature, the RI of many physical quantities varies within this range 1.4–1.8 RIU or 1.5–2.2 RIU, including but not limited to the methane: 1.4478–1.4364 RIU [46], enamel: 1.631 ± 0.007 RIU [47], polystyrene: 1.54–1.59 RIU [48], and NaCl solutions: 1.446–1.458 RIU [49]. Thus, the MWS can be applied widely to multiple physical scenarios. For instance, it is important to know the concentration of the explosive methane in a mine

at all times. Also, workers in a salt farm need to know the concentration of NaCl solution to control the timing of a chemical process. Various other physical scenarios are not mentioned here. In Supplemental Material Section I, a specific method for detecting methane gas concentration is given. Additionally, the conventional GH devices mainly depend on the amplitude modulation (AM) mode, which may produce superior detection accuracy but a low and discrete detection window as well as a lack of stability. In contrast, the suggested design is based on frequency modulation (FM), namely, through detecting the shift of the peak LS (f_p) concerning the changes of physical quantities to be detected. Despite being primarily concerned with FM mode, this work may also be utilized in the AM mode. For the detailed information on the performance of the detector settings and comparing it with some current typical sensor designs, it is possible to specifically refer to Table I at the end of the context. Because of the uniqueness of the principle and structure construction, the MWS structure could be reasonably expanded to the application of the detecting device in terms of the displacement, temperature, and even specific plasma magnetic field via modifying the content material or structure of "N_x" [50], [51], [52], and all the expansions are predicted to attain dual-sensitivity detecting characteristics, which furnishes an essential reference to the design of the GH detecting device and provides a simple implementation idea for the nonreciprocal passive devices.

The transfer matrix method and the stationary phase method are combined in this research to streamline the analysis of multilayer metal–dielectric systems, which have proven reliable for the design [53]. All calculation results in the research are based on MATLAB.

II. Theoretical Model

Fig. 1 depicts the structure of the proposed detector together with the GH effect caused by the electromagnetic waves (EWs) that are incident from behind at the surface. The forward operating scenario is sketched lightly but follows the same coordinate system as the backward. The proposed structure is composed of a periodic stack of dielectric and metal layers in a certain way. Considering their potential to deliver the desired performance and the fabrication and cost, silicon (Si) and silver are selected as the primary constituent materials for the device. Moreover, the materials offer potential advantages for silicon-based photonics. The forward incidence of the structure could be described as "$(SA)^2N_x(AS)^3$," where A and N_x, respectively, denote the silver layer and the layer to be detected, and layer S refers to the silicon layer. It should be noted that all parameter designs are the result of balancing device performance. While designing this structure, it was found that only ideal nonreciprocal dual-sensitivity characteristic is exhibited under the conditions of the proposed thickness and layer settings, which means that there is a certain level of ingenuity required in setting the number of layers in the structure. Similarly, the backward one could be denoted as "$(SA)^3N_x(AS)^2$." To clarify the proposed structure, the names of the dielectrics are directly used to indicate the composition of the structure in Fig. 1.

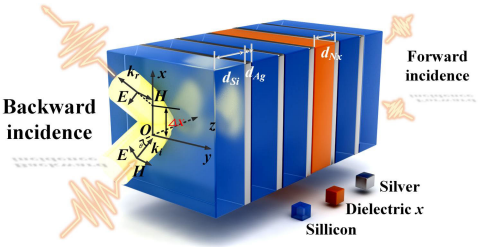

Fig. 1. Schematic plot of the presented MWS detector with the GH shift produced by the incident EWs from forward and backward, respectively.

The settings individually are selected by weighing the sensors' performance indicators: $d_{Si} = 250$ nm, $d_{Ag} = 35$ nm, and $d_{Nx} = 225$ nm. The RI of the silicon in the working frequency (f) is set as 3.43 [54] and that of N_x is denoted as n_x. Besides, the dielectric function and the RI of the silver are represented by the Drude–Lorentz model [55]

$$\varepsilon_r = \varepsilon_\infty - \frac{\omega_p^2}{\omega^2 + i\omega\gamma} - \frac{\Delta\Omega^2}{(\omega^2 - \Omega^2) + i\zeta}, \quad n_A = \sqrt{\varepsilon_r} \tag{1}$$

where $\omega = 2\pi f$, $\omega_p = 2\pi \times 2214.6 \times 10^{12}$ Hz is the plasma frequency, $\gamma = 2\pi \times 4.8 \times 10^{12}$ Hz denotes the frequency of the collision, $\Delta = 1.6604$ represents the Lorentz item weight, $\Omega = 2\pi \times 1330.1 \times 10^{12}$ Hz signifies the Lorentz harmonic intensity, and $\zeta = 2\pi \times 620.7 \times 10^{12}$ is the vibration spectrum width.

The transfer matrix approach could be employed for multilayer media to derive the suggested structure's EWs transmission characteristics by applying time-dependent Maxwell's equations. The matrix of the silver and the dielectrics can be computed as follows:

$$\mathbf{M}_i = \begin{bmatrix} \cos\xi_i & -i/\eta_i \sin\xi_i \\ -i\eta_i \sin\xi_i & \cos\xi_i \end{bmatrix} \quad (i = \mathrm{S},\ \mathrm{A},\ \mathrm{N_x}) \tag{2}$$

where $\eta_i = (\varepsilon_0/\mu_0)^{1/2} \cdot n_i/\cos\theta_i$ adapts for the EWs under the transverse magnetic (TM) mode, while $\eta_i = (\varepsilon_0/\mu_0)^{1/2} \cdot n_i \cdot \cos\theta_i$ is under the transverse electric (TE) mode, and $\xi_i = n_i \cdot d_i \cdot \cos\theta_i$. It should be noted that the RI of air $n_0 = 1$, so the wave impedance in air η_0 could be obtained. The TM wave serves as the foundation for all topics in this work, demonstrating that the structure is polarization-insensitive. In addition, the parameters d_i and θ_i introduce the thickness and the incident angle of layer i. θ_0 denotes the incident angle from the air.

The following equation can be used to represent the correlation between the electric and magnetic fields of the MWS structure with L layers:

$$\begin{pmatrix} E_1 \\ H_1 \end{pmatrix} = \mathbf{M}_{\mathrm{Forward\,(Backward)}} \cdot \begin{pmatrix} E_{L+1} \\ H_{L+1} \end{pmatrix} \tag{3}$$

and the suggested structure's whole transfer matrix may be expressed as

$$\begin{aligned} \mathbf{M}_{\mathrm{Forward\,(Backward)}} &= (\mathbf{M_S M_A})^{2(3)} \mathbf{M_{N_x}} (\mathbf{M_A M_S})^{3(2)} \\ &= \begin{pmatrix} \Gamma_{11} & \Gamma_{12} \\ \Gamma_{21} & \Gamma_{22} \end{pmatrix}. \end{aligned} \tag{4}$$

For the convenience of presenting the expression of the reflection coefficient, (3) could be transformed into the following equation:

$$\begin{pmatrix} E_{i,1}+E_{r,1} \\ \eta_1(E_{i,1}-E_{r,1}) \end{pmatrix} = \begin{pmatrix} \Gamma_{11} & \Gamma_{12} \\ \Gamma_{21} & \Gamma_{22} \end{pmatrix} \begin{pmatrix} E_{\mathrm{t,L+1}} \\ \eta_{\mathrm{L+1}} E_{\mathrm{t,L+1}} \end{pmatrix} \quad (5)$$

where $E_{\mathrm{i},1}$ and $E_{\mathrm{r},1}$ denote the amplitudes of the incident and reflected EWs before interface 1. Accordingly, $E_{\mathrm{i,L+1}}$ and $E_{\mathrm{r,L+1}}$ signify the amplitudes of the incident and reflected EWs after interface L + 1. Since all discussions of the structure assume that it is immersed in air, thus $\eta_1 = \eta_{\mathrm{L+1}} = \eta_0$. Therefore, the reflection coefficient may be calculated as a result as [56]

$$r = \frac{\Gamma_{11}\eta_0 + \Gamma_{12}\eta_0^2 - \Gamma_{21} - \Gamma_{22}\eta_0}{\Gamma_{11}\eta_0 + \Gamma_{12}\eta_0 + \Gamma_{21} + \Gamma_{22}\eta_0^2}. \quad (6)$$

The wave vectors of the incident and reflected EWs are shown in Fig. 1 by $k_{\mathbf{i}}$ and $k_{\mathbf{r}}$, respectively. The GH effect that manifested itself on the surface of the suggested structure is indicated by the LS value $\Delta\mathrm{X}$ (λ). It is worth noting that there are numerous formulas for calculating the GH effect as the perpendicular distance between the ideal and actual emitted rays. In this case, a different expression for the GH effect, namely, the distance of the emitted point relative to the incident point, is utilized, proving more suitable for calculating the FM mode. Aside from it, the incident EWs are considered to be Gaussian wave packets with normalized characteristic lengths of $\Delta k_{\mathbf{x}}/k_{\mathbf{x}}$ ($\Delta k_{\mathbf{x}} \ll k_{\mathbf{x}}$). When the reflection occurs, an LS is produced, and the value leveraging the stationary phase approach may be stated as [57]

$$\Delta\mathrm{X} = \frac{\partial\psi}{\partial k_x}, \quad \psi = \arctan\frac{\mathrm{Im}(r)}{\mathrm{Re}(r)} \quad (7)$$

where ψ signifies the phase change of the reflected EWs relative to the incident, and k_x stands for the x-component of the wavevector. Im (r) and Re (r) are the imaginary and real components of the reflection coefficient r, and (6) may be employed to get access to the surface reflection coefficient of the proposed structure.

III. Numerical Results and Discussion

When it is perplexing to determine a physical quantity directly, a certain structure is suggested to convert its fluctuation into an observable one. The amount of the unknown physical quantity within a specified measurement range may be determined by leveraging a precise mathematical connection. This is the fundamental principle behind how sensors operate. The FM, one of the essential and deployed elements of the sensor implementation method, is utilized in this study, where f_p serves as a probe for the fluctuation of the RI to be detected.

The physical operation of the device and its sensing parameters will be thoroughly discussed in the following parts. Beforehand, for a quantitative description of the talent of the argued device, the following parameters must be introduced antecedently [58]:

$$\text{Quality factor (Q)} = \frac{f_p}{\mathrm{FWHM}}, \quad \text{Sensity (S)} = \frac{\Delta f_p}{\Delta RI}$$

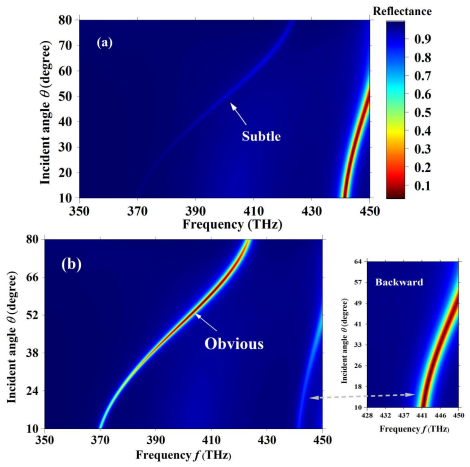

Fig. 2. Diagrams of reflectance relative to the angle of incidence and frequency for EWs incident on (a) front and (b) rear surfaces of the structure in the operating frequency when n_x is equal to 1.5.

$$\text{Figure of merit (FOM)} = \frac{\mathrm{S}}{\mathrm{FWHM}}$$
$$\text{Detection limit (DL)} = \frac{f_p}{20\mathrm{SQ}}. \quad (8)$$

Starting with Fig. 2, it is evident that the recommended structure enjoys a fantastic nonreciprocal reflection effect at the operating frequency. The majority of the incident EWs at a specific incident angle will be reflected, and merely, two reflectivity troughs appear at the specific frequency. Although the two reflectivity minimal values could be discerned, their magnitudes of them are distinct, which is the most significant nonreciprocal phenomenon. Furthermore, the second nonreciprocal feature that merits attention is that the frequency shift rates of the reflectivity minima in the front and back incidence vary concerning the incident angle. Ordinarily, the reflection phase would change more steeply when the reflectivity declines dramatically. Thus, the nonreciprocal effects serve as a crucial basis and prerequisite for the GH effect that will be covered later.

Why would it cause such a nonreciprocal phenomenon when the incident EWs are incident so differently? To facilitate the explanation of the causes of the phenomenon, Fig. 3(a)–(e) is introduced. The structure's absorption and reflectance curves at a 20° incident angle are displayed in Fig. 3(a). It is not perplexing to determine that the structure generates double absorption peaks: one is at $f = 443.4$ THz for the backward incidence, which corresponds to a reflectance trough with the value of 0.56 at 443.4 THz, and the other one is at $f = 374.7$ THz for the forward incidence, which corresponds to an absorption of roughly 0.4 at 374.7 THz.

In the entire structure, silver is the only lossy medium. Therefore, when discussing absorption, attention should be paid to the energy distribution around the silver film. For the front incidence in Fig. 3(b), when $f = 374.7$ THz, it is discerned that a slight field is localized in layer S, while the magnetic field components H_y are concentrated primarily in layer $\mathrm{N_x}$. Especially at the junction of $\mathrm{N_x}$ and silver, the normalized magnetic field is at its maximum, reaching 11.1. For the forward incidence, the $\mathrm{N_x}$ layer and the silver metal

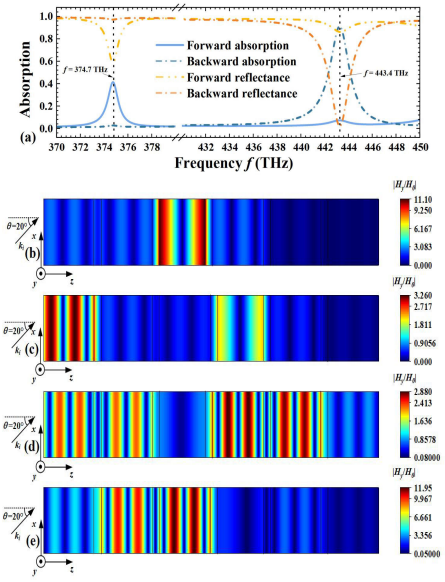

Fig. 3. When $\theta = 20°$ and $n_X = 1.5$, (a) plot of both absorption and reflectance curves for the forward and backward incidence, the magnetic field relative intensity distribution diagrams of the structure at the frequency of 374.7 THz for (b) forward and (c) backward, and the displays at the frequency equal to 443.4 THz for (d) forward and (e) backward.

adhering to N_x form a microcavity, with N_x serving as the cavity and silver as the mirror. This microcavity has been found to have a localized effect on EWs at 374.7 THz. Due to the lossy characteristics of silver, the EWs are absorbed when they come into contact with the mirror, forming an absorption peak in the spectrum. When it comes to the backward incidence in Fig. 3(c), it is apparent the ability of N_x to localize the electromagnetic field decreases and the maximum normalized magnetic field in N_x is only around 2. The majority of the energy is blocked in the first S layer. Since it does not have sufficient contact with other silver media in the structure, the absorption that is manifested is also relatively weak. In terms of 443.4 THz for the forward incidence, as depicted in Fig. 3(d), although the microcavities comprising silver layers and layer S restrict some magnetic fields, it numerically turns out to be relatively slight that the maximum intensity is only around 2.88 in the layer S, resulting in similarly weak absorption. For the backward in Fig. 3(e), it is discerned that the microcavities comprising silver layers and layer S, which initially was not strongly localized, generate a substantial magnetic field localization, where the normalized magnetic field attains 11.95. As a result, great absorption occurs at such frequency.

In general, the presence of microcavities induces absorption properties at specific frequencies. The ingenious asymmetry of the structure makes the absorption rates in the forward and backward directions differ significantly, so that the nonreciprocal properties are obtained at the macroscopic level.

As found in Fig. 4(a) and (b), a direct outcome of such nonreciprocal absorption reflectance valleys is a dramatic alternation in the reflection phase, one of the most direct causes of the enhanced GH effect.

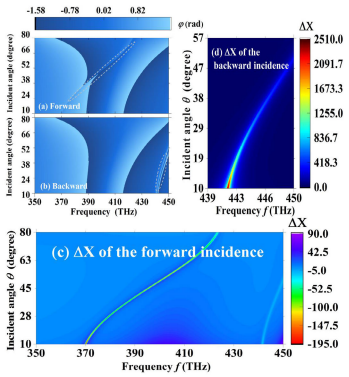

Fig. 4. Figures of the reflection phase versus frequency and incident angle for (a) forward and (b) backward incidence conditions and their corresponding GH LS plots for (c) front and (d) back.

For the forward incidence, as shown in Fig. 4(a), a sharp dividing line exists in the frequency band from about 370 to 420 THz (circled in white dashed lines). In light of (6), the partial derivative of the phase concerning the incident wave frequency determines how significant the GH effect is. Thus, a giant GH effect is generated around the dividing line. A comparable GH effect is produced by the backward incidence at around 440 THz, but at the original forward location, the GH effect essentially does not exist, which agrees well with Fig. 2. However, the difference between the positive and negative LS values produced by the forward and backward directions is another intriguing feature. In the subsequent discussion, if not specified, the default is to indicate its absolute value out of the convenience of explanation.

Considering the abovementioned nonreciprocal effect, we readily link this structure to the application as a nonreciprocal RI sensor. Afterward, we will go into more depth about this intriguing sensing structure.

Combining Fig. 5(a) and (c), it is evident that when the sensor operates forward, it theoretically can detect substances with an RI ranging from 1.4 to 1.8. The result of the linear fit to the function is calculated as $f_p = -197.65\text{RI} + 671.73$, with the sensitivity equal to 197.65 THz/RIU, and the R-square is 0.9919. For the backward mode, the linear range comes from 1.5 to 2.1, with the linear function as $f_p = -2.374\text{RI} + 446.23$. The sensitivity is 2.374 THz/RIU, and the R-square equals 0.9945. Due to the relationship between the concentration of many substances and their RI, their concentrations can be reflected by the RI. In Supplemental Material Section I, we provide a theoretical application to illustrate this concept. So, it is learned from the calculation results that the nonreciprocally dual sensitivity sensor is implemented. The generation process of the nonreciprocal absorption has previously been examined. However, these analyses are focused on the fixed state situation of $n_x = 1.5$ and could not explain the reason why the sensitivity of the forward and backward incidence is different, which necessitates a few words of extra clarification in the following.

As mentioned in Fig. 3, the photon localization leads to significant absorption at different frequencies due to distinct microcavities, and the unique asymmetric nature of the structure leads to the incident EWs localization in the layer

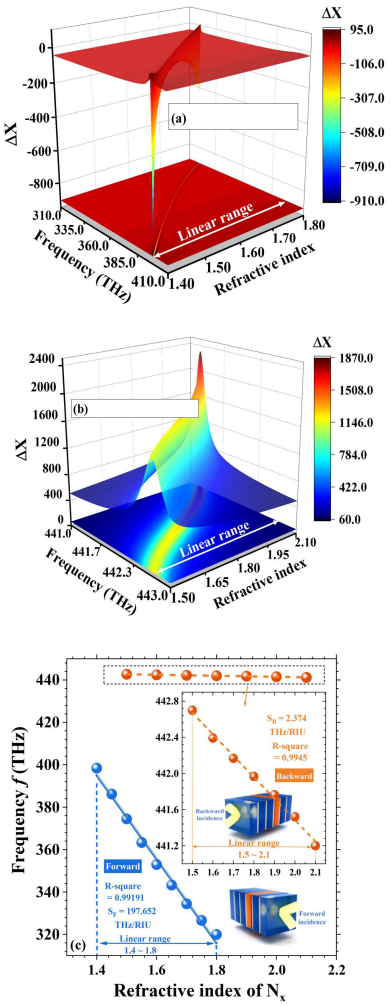

Fig. 5. Plots of LS extreme value shown against the RI of N_X and frequency for (a) forward and (b) backward. (c) Diagram of the linear fits for both forward and backward.

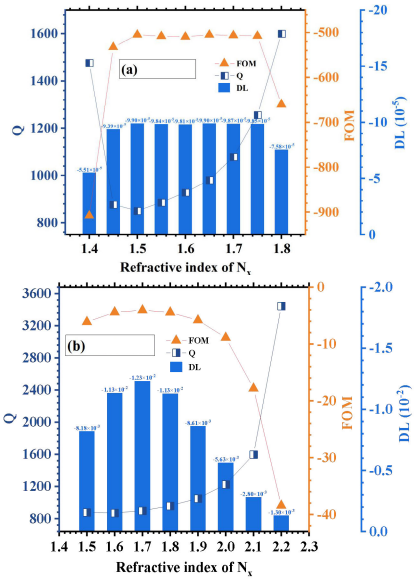

Fig. 6. *Q*, FOM, and DL of the sensing structure for (a) forward incident EWs and (b) backward.

N_X at forwarding incidence, and such microcavity coupling frequencies transform as the n_x changes. A more empathetic sensing performance is displayed because of the responsive feature of alternating the coupling mode to the changes of RI. Nevertheless, for the backward, since photons are primarily localized at layer S, where their RI is constant, altering n_x at this point would require modifying the transport characteristics of the MWS structure. It only slightly impacts the initial photon localization, which brings a low sensitivity for the backward operating mode.

For a more comprehensive display of the performance of the proposed sensors, Fig. 6(a) and (b) is provided. To begin with the forward condition, we discover that when n_x rises, Q first generates an extreme value of approximately 1480 at $n_x = 1.4$ and then drops suddenly. Afterward, an exhibition of an upward trend is shown with a slow, but steady rate of change until n_x is equal to 1.8, at which point it achieves a maximum value of around 1600. Accordingly, there is an opposite trend for the FOM and the DL. The minimal DL value of 5.51×10^{-5} and 7.58×10^{-5} may be attained in forwarding incidence mode at $n_x = 1.4$ and 1.8, respectively. Additionally, the sensor enjoys consistent detection performance, varying about 9.9×10^{-5}, between 1.45 and 1.75. These imply excellent performance in the forward mode.

For the backward mode, notwithstanding that the sensitivity has been proven to be relatively low in comparison to forward incidence, the more comprehensive sensing range and the substantially larger LS value of the GH effect have a role as the key benefits of the backward operating mode. Combining Figs. 4(d) and 6(b), it is discovered that the backward incidence has a higher GH value at a specific RI, and the generation of the higher GH value implies the experimental accuracy requirements of the device to detect the LS is significantly reduced.

The backward mode allows it to adapt to physical scenarios that require a wide detection range without excessive accuracy. Numerically, to start with $n_x = 1.5$, Q and FOM remain low, with the DL value of 0.00818. Immediately after it, there exists a little increase in the DL, i.e., 0.0123, and then, it steadily drops. Significantly, the region between 2.1 and 2.2 is where the Q value rises most quickly and where the FOM changes mainly, indicating a superior sensing performance around that range. More specifically, for our proposed device, the detection limit is sufficient for detecting methane content when operating in forward mode when the methane-sensitive film is added to the position of the layer N_X [59]. When operating in the backward mode, the proposal is enabled to detect the RI of unknown materials at a specified frequency [55].

It is vital to talk about how the thicknesses of the dielectric layers affect the performance of the sensor because the actual manufacture of the sensor frequently results in certain inevitable faults. Supplemental Material Section II offers a more detailed explanation of how errors in the RI of the S layers and the thickness of N_X can affect the detection performance.

As depicted in Fig. 7(a)–(c), the peak value decreases from 282.06λ to 18.07λ as d_{Ag} increases at 5-nm intervals, which indicates that the performance of sensing decreases as the

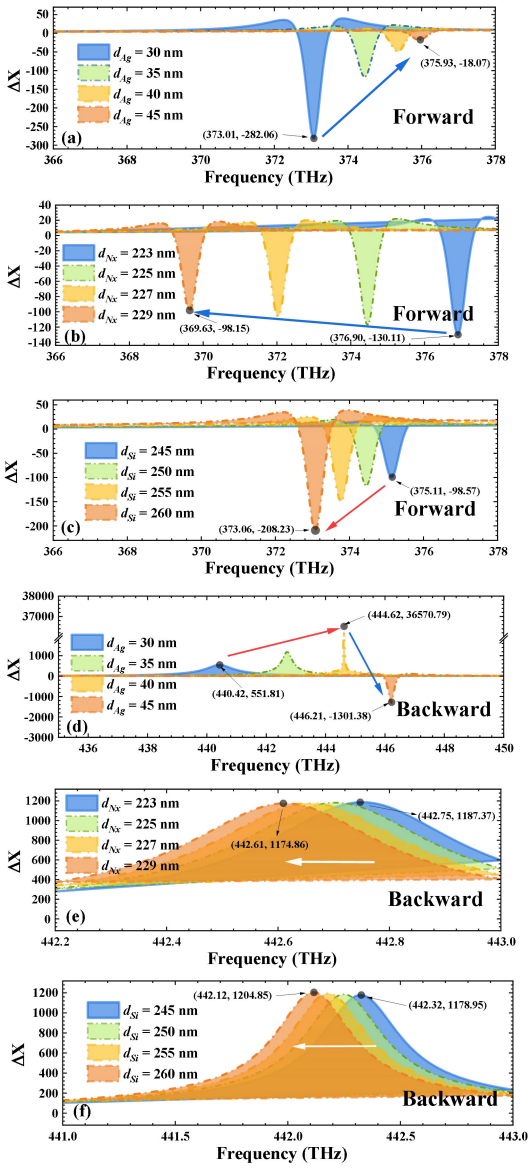

Fig. 7. When the incident angle is 20° and $n_X = 1.5$, the plots of the impacts of the variation of the thicknesses of layers (a) A, (b) N_x, and (c) S on the forward peak GH LS within the operating frequency, and the diagrams of the effects of the alternation of the thicknesses of layers (d) A, (e) N_x, and (f) S on the backward peak GH LS within the operating frequency.

silver layer becomes thicker, so special attention must be paid to the control of silver layer thickness in actual manufacturing. Since the influence of layer N_x on the GH, the peak value is relatively faint, and it only ignites the redshift of the frequency position. Therefore, the effect on sensor performance is also negligibly small. This enables the N_x layer's application to other functional materials to be considerably more adaptable and fault-tolerant. For layer S, with the thickness increasing by 5 nm, the LS will transform from 98.57λ to 208.23λ, which is relatively steady and predictable.

For the backward incidence, both layer N_x and layer S exhibit weaker impacts on the sensing performance—there are only a few wavelength alternations in the values, and the frequency position changes are relatively weak, but layer A enjoys a very noticeable influence on the peak LS, and after the critical value, the GH effect will switch from being positive to negative, from 36570.79λ to -1301.38λ, which is an intriguing occurrence.

TABLE I
COMPARISON WITH OTHER RI SENSORS BASED ON THE GH EFFECT

Refs.	Measuring range (RIU)	Sensitivity	Quality factor	Multi-sensitivity and multi-range
[60]	1~ 1.00015	1.27×10^7 mm/RIU	84000	None
[61]	1~ 1.0001	3.58×10^6 μm/RIU	10000	None
[62]	1.4 ~ 2.6	0.42 THz/RIU	815.56	None
Present work	Forward:1.4 ~1.8 Backward:1. 5~2.2	Forward:197.652 THz/RIU Backward:2.374 THz/RIU	1600	Yes

Table I compares different sensors based on the GH effect. Apparently, this work does not show a significant improvement in terms of the Q factor and sensitivity compared to the results in [62], but it is still better. With an order of magnitude increase in both indicators, moreover, this study takes a significant lead in terms of the RI measurement range and is capable of performing measurements across multiple ranges. This outstanding performance is several orders of magnitude better than the results presented in [60] and [61], showcasing its superiority and advancements in this field.

IV. CONCLUSION

To conclude, a novel concept of the MWS detecting device based on the reflected GH effect containing metal layers is displayed in this work. The absorption of the proposal of the forward and backward incident EWs results in a massive reflected GH effect, certainly in the near-infrared band, due to the asymmetric introduction of the topological defect to the MWS structure. The distinct microcavity modes under reverse incidence directions bring a significant nonreciprocal phenomenon in both forward and backward directions. The local address of the photon energy at the resonance of the different incident modes will be significantly out of alignment due to the asymmetry, in conjunction with a singular sensibility to the fluctuation of the defect layer. Given this, the detecting performance of the device in terms of RI is considered, and the numerical results show that the sensitivity in the forward mode is about 197.652 THz/RIU, while 2.374 THz/RIU for the backward. The DL could reach as low as 5.51×10^{-5} with a linear range from 1.4 to 1.8 for the forward and 1.3×10^{-3} with a linear range from 1.5 to 2.2 for the backward. The simplicity of the construction of the novel MWS structure and the high non-reciprocal detecting performance make it feasible for multiphysics scenarios and could be expanded to more application scenarios by adding functional materials. These features furnish an essential reference to the development of GH sensors and integration technologies.

REFERENCES

[1] F. Goos and H. Hänchen, "Ein neuer und fundamentaler versuch zur totalreflexion," *Annalen Physik*, vol. 436, nos. 7–8, pp. 333–346, Jan. 1947, doi: 10.1002/andp.19474360704.

[2] F. Goos and H. Lindberg-Hänchen, "Neumessung des strahlversetzungseffektes bei totalreflexion," *Annalen Physik*, vol. 440, nos. 3–5, pp. 251–252, Jan. 1949, doi: 10.1002/andp.19494400312.

[3] M. A. Porras, "Moment-method evaluation of the angular and lateral shifts of reflected light beams," *Opt. Commun.*, vol. 131, no. 1, pp. 13–20, Oct. 1996.

[4] M. Merano, A. Aiello, M. P. van Exter, and J. P. Woerdman, "Observing angular deviations in the specular reflection of a light beam," *Nature Photon.*, vol. 3, no. 6, pp. 337–340, Jun. 2009, doi: 10.1038/nphoton.2009.75.

[5] Y. Aharonov, D. Z. Albert, and L. Vaidman, "How the result of a measurement of a component of the spin of a spin-1/2 particle can turn out to be 100," *Phys. Rev. Lett.*, vol. 60, no. 14, pp. 1351–1354, Apr. 1988, doi: 10.1103/PhysRevLett.60.1351.

[6] I. J. Singh and V. P. Nayyar, "Lateral displacement of a light beam at a ferrite interface," *J. Appl. Phys.*, vol. 69, no. 11, pp. 7820–7824, Jun. 1991, doi: 10.1063/1.347512.

[7] N. Goswami, A. Kar, and A. Saha, "Long range surface plasmon resonance enhanced electro-optically tunable Goos–Hänchen shift and Imbert–Fedorov shift in ZnSe prism," *Opt. Commun.*, vol. 330, pp. 169–174, Nov. 2014, doi: 10.1016/j.optcom.2014.05.042.

[8] H. Wu, Q. Luo, H. Chen, Y. Han, X. Yu, and S. Liu, "Magnetically controllable nonreciprocal Goos–Hänchen shift supported by a magnetic plasmonic gradient metasurface," *Phys. Rev. A, Gen. Phys.*, vol. 99, no. 3, Mar. 2019, Art. no. 033820, doi: 10.1103/PhysRevA.99.033820.

[9] I. V. Shadrivov, A. A. Zharov, and Y. S. Kivshar, "Giant Goos–Hänchen effect at the reflection from left-handed metamaterials," *Appl. Phys. Lett.*, vol. 83, no. 13, pp. 2713–2715, Sep. 2003, doi: 10.1063/1.1615678.

[10] D.-K. Qing and G. Chen, "Goos–Hänchen shifts at the interfaces between left- and right-handed media," *Opt. Lett.*, vol. 29, no. 8, p. 872, 2004, doi: 10.1364/ol.29.000872.

[11] R. Talebzadeh and A. Namdar, "Positively and negatively large Goos–Hänchen lateral displacements from a single negative layered structure," *Appl. Opt.*, vol. 51, no. 27, p. 6484, Sep. 2012, doi: 10.1364/AO.51.006484.

[12] R. W. Ziolkowski, "Pulsed and CW Gaussian beam interactions with double negative metamaterial slabs," *Opt. Exp.*, vol. 11, no. 7, p. 662, Apr. 2003, doi: 10.1364/OE.11.000662.

[13] L.-G. Wang and S.-Y. Zhu, "Large negative lateral shifts from the Kretschmann–Raether configuration with left-handed materials," *Appl. Phys. Lett.*, vol. 87, no. 22, Nov. 2005, Art. no. 221102, doi: 10.1063/1.2136225.

[14] X. Li, P. Wang, F. Xing, X.-D. Chen, Z.-B. Liu, and J.-G. Tian, "Experimental observation of a giant Goos–Hänchen shift in graphene using a beam splitter scanning method," *Opt. Lett.*, vol. 39, no. 19, p. 5574, 2014, doi: 10.1364/OL.39.005574.

[15] M. Cheng et al., "Spatial and angular shifts of terahertz wave for the graphene metamaterial structure," *J. Phys. D, Appl. Phys.*, vol. 48, no. 28, Jul. 2015, Art. no. 285105, doi: 10.1088/0022-3727/48/28/285105.

[16] Y. Chen, Y. Ban, Q.-B. Zhu, and X. Chen, "Graphene-assisted resonant transmission and enhanced Goos–Hänchen shift in a frustrated total internal reflection configuration," *Opt. Lett.*, vol. 41, no. 19, p. 4468, Oct. 2016, doi: 10.1364/OL.41.004468.

[17] H. M. Lai and S. W. Chan, "Large and negative Goos–Hänchen shift near the Brewster dip on reflection from weakly absorbing media," *Opt. Lett.*, vol. 27, no. 9, p. 680, May 2002, doi: 10.1364/OL.27.000680.

[18] L.-G. Wang, H. Chen, and S.-Y. Zhu, "Large negative Goos–Hänchen shift from a weakly absorbing dielectric slab," *Opt. Lett.*, vol. 30, no. 21, p. 2936, Nov. 2005, doi: 10.1364/OL.30.002936.

[19] A. Madani and S. R. Entezar, "Tunable enhanced Goos–Hänchen shift in one-dimensional photonic crystals containing graphene monolayers," *Superlattices Microstruct.*, vol. 86, pp. 105–110, Oct. 2015, doi: 10.1016/j.spmi.2015.07.042.

[20] Y. Cao, Y. Fu, Q. Zhou, Y. Xu, L. Gao, and H. Chen, "Giant Goos–Hänchen shift induced by bounded states in optical PT-symmetric bilayer structures," *Opt. Exp.*, vol. 27, no. 6, p. 7857, Mar. 2019, doi: 10.1364/OE.27.007857.

[21] X. Yin, L. Hesselink, Z. Liu, N. Fang, and X. Zhang, "Large positive and negative lateral optical beam displacements due to surface plasmon resonance," *Appl. Phys. Lett.*, vol. 85, no. 3, pp. 372–374, Jul. 2004, doi: 10.1063/1.1775294.

[22] L. Chen, X. Liu, Z. Cao, and S. Zhuang, "Mechanism of giant Goos–Hänchen effect enhanced by long-range surface plasmon excitation," *J. Opt.*, vol. 13, no. 3, Jan. 2011, Art. no. 035002, doi: 10.1088/2040-8978/13/3/035002.

[23] L. Salasnich, "Enhancement of four reflection shifts by a three-layer surface-plasmon resonance," *Phys. Rev. A, Gen. Phys.*, vol. 86, no. 5, Nov. 2012, Art. no. 055801, doi: 10.1103/PhysRevA.86.055801.

[24] L.-G. Wang and S.-Y. Zhu, "Giant lateral shift of a light beam at the defect mode in one-dimensional photonic crystals," *Opt. Lett.*, vol. 31, no. 1, p. 101, Jan. 2006, doi: 10.1364/OL.31.000101.

[25] D. Zhao, D. Zhong, Y. Hu, S. Ke, and W. Liu, "Imaginary modulation inducing giant spatial Goos–Hänchen shifts in one-dimensional defective photonic lattices," *Opt. Quantum Electron.*, vol. 51, no. 4, pp. 1–12, Mar. 2019, doi: 10.1007/s11082-019-1828-6.

[26] X. Liu, Z. Cao, P. Zhu, Q. Shen, and X. Liu, "Large positive and negative lateral optical beam shift in prism-waveguide coupling system," *Phys. Rev. E, Stat. Phys. Plasmas Fluids Relat. Interdiscip. Top.*, vol. 73, no. 5, May 2006, Art. no. 056617, doi: 10.1103/PhysRevE.73.056617.

[27] L. Chen, Z. Cao, F. Ou, H. Li, Q. Shen, and H. Qiao, "Observation of large positive and negative lateral shifts of a reflected beam from symmetrical metal-cladding waveguides," *Opt. Lett.*, vol. 32, no. 11, p. 1432, Jun. 2007, doi: 10.1364/OL.32.001432.

[28] X. Liu, Q. Yang, Z. Qiao, T. Li, P. Zhu, and Z. Cao, "Physical origin of large positive and negative lateral optical beam shifts in prism–waveguide coupling system," *Opt. Commun.*, vol. 283, no. 13, pp. 2681–2685, Jul. 2010, doi: 10.1016/j.optcom.2010.03.002.

[29] D. Felbacq, A. Moreau, and R. Smaâli, "Goos–Hänchen effect in the gaps of photonic crystals," *Opt. Lett.*, vol. 28, no. 18, p. 1633, Sep. 2003, doi: 10.1364/OL.28.001633.

[30] K. V. Sreekanth, S. Han, and R. Singh, "$Ge_2Sb_2Te_5$-based tunable perfect absorber cavity with phase singularity at visible frequencies," *Adv. Mater.*, vol. 30, no. 21, Apr. 2018, Art. no. 1706696, doi: 10.1002/adma.201706696.

[31] K. V. Sreekanth, Q. Ouyang, S. Han, K.-T. Yong, and R. Singh, "Giant enhancement in Goos–Hänchen shift at the singular phase of a nanophotonic cavity," *Appl. Phys. Lett.*, vol. 112, no. 16, Apr. 2018, Art. no. 161109, doi: 10.1063/1.5027133.

[32] K. V. Sreekanth et al., "Generalized Brewster angle effect in thin-film optical absorbers and its application for graphene hydrogen sensing," *ACS Photon.*, vol. 6, no. 7, pp. 1610–1617, Jul. 2019, doi: 10.1021/acsphotonics.9b00564.

[33] K. V. Sreekanth, P. Mahalakshmi, S. Han, M. S. M. Rajan, P. K. Choudhury, and R. Singh, "Brewster mode-enhanced sensing with hyperbolic metamaterial," *Adv. Opt. Mater.*, vol. 7, no. 21, Aug. 2019, Art. no. 1900680, doi: 10.1002/adom.201900680.

[34] H. Ma and R.-X. Wu, "Enhancing the nonreciprocal Goos–Hänchen shift by the Fano resonance of coupled gyromagnetic chains at normal incidence," *Opt. Exp.*, vol. 30, no. 26, p. 46031, Dec. 2022, doi: 10.1364/OE.474217.

[35] R. D. Meade, K. D. Brommer, A. M. Rappe, and J. D. Joannopoulos, "Electromagnetic Bloch waves at the surface of a photonic crystal," *Phys. Rev. B, Condens. Matter*, vol. 44, no. 19, pp. 10961–10964, Nov. 1991, doi: 10.1103/PhysRevB.44.10961.

[36] M. Xiao, Z. Q. Zhang, and C. T. Chan, "Surface impedance and bulk band geometric phases in one-dimensional systems," *Phys. Rev. X*, vol. 4, no. 2, Apr. 2014, Art. no. 021017, doi: 10.1103/PhysRevX.4.021017.

[37] Y.-C. Lin, S.-H. Chou, and W.-J. Hsueh, "Robust high-Q filter with complete transmission by conjugated topological photonic crystals," *Sci. Rep.*, vol. 10, no. 1, p. 7040, Apr. 2020, doi: 10.1038/s41598-020-64076-3.

[38] Y. Tsurimaki et al., "Topological engineering of interfacial optical Tamm states for highly sensitive near-singular-phase optical detection," *ACS Photon.*, vol. 5, no. 3, pp. 929–938, Mar. 2018, doi: 10.1021/acsphotonics.7b01176.

[39] F. Wu et al., "Giant enhancement of the Goos–Hänchen shift assisted by quasibound states in the continuum," *Phys. Rev. Appl.*, vol. 12, no. 1, Jul. 2019, Art. no. 014028, doi: 10.1103/PhysRevApplied.12.014028.

[40] M. Idrees, M. Ullah, and L.-G. Wang, "Enhancement of the Goos–Hänchen shift via chiral quantum-dot molecule systems," *Phys. Rev. A, Gen. Phys.*, vol. 108, no. 1, Jul. 2023, Art. no. 013701, doi: 10.1103/PhysRevA.108.013701.

[41] W. Kong, Y. Wan, S. Li, W. Zhao, and Z. Zheng, "High-sensitivity Goos–Hänchen shift sensing based on Bloch surface wave," *Sens. Actuators A, Phys.*, vol. 276, pp. 62–67, Jun. 2018, doi: 10.1016/j.sna.2018.04.017.

[42] Z. Liu, F. Lu, L. Jiang, W. Lin, and Z. Zheng, "Tunable Goos–Hänchen shift surface plasmon resonance sensor based on graphene-hBN heterostructure," *Biosensors*, vol. 11, no. 6, p. 201, Jun. 2021, doi: 10.3390/bios11060201.

[43] T. Yu, H. Li, Z. Cao, Y. Wang, Q. Shen, and Y. He, "Oscillating wave displacement sensor using the enhanced Goos–Hänchen effect in a symmetrical metal-cladding optical waveguide," *Opt. Lett.*, vol. 33, no. 9, p. 1001, May 2008, doi: 10.1364/OL.33.001001.

[44] X. Wang et al., "High-sensitivity temperature sensor using the ultrahigh order mode-enhanced Goos–Hänchen effect," *Opt. Exp.*, vol. 21, no. 11, p. 13380, Jun. 2013, doi: 10.1364/OE.21.013380.

[45] M. Hedhly, Y. Wang, S. Zeng, F. Ouerghi, J. Zhou, and G. Humbert, "Highly sensitive plasmonic waveguide biosensor based on phase singularity-enhanced Goos–Hänchen shift," *Biosensors*, vol. 12, no. 7, p. 457, Jun. 2022, doi: 10.3390/bios12070457.

[46] H. Liu, C. Chen, Y. Zhang, B. Bai, and S. Tang, "A high-sensitivity methane sensor with localized surface plasmon resonance behavior in an improved hexagonal gold nanoring array," *Sensors*, vol. 19, no. 21, p. 4803, Nov. 2019, doi: 10.3390/s19214803.

[47] Z. Meng et al., "Measurement of the refractive index of human teeth by optical coherence tomography," *J. Biomed. Opt.*, vol. 14, no. 3, Jun. 2009, Art. no. 034010, doi: 10.1117/1.3130322.

[48] C. Smart and E. Willis, "Determination of refractive indices of polystyrene latices by light scattering," *J. Colloid Interface Sci.*, vol. 25, no. 4, pp. 577–583, Dec. 1967, doi: 10.1016/0021-9797(67)90071-9.

[49] V. Mishra, "Refractive index and concentration sensing of solutions using mechanically induced long period grating pair," *Opt. Eng.*, vol. 44, no. 9, Sep. 2005, Art. no. 094402, doi: 10.1117/1.2054627.

[50] Y.-T. Xiang, B.-F. Wan, and H.-F. Zhang, "Multiscale and multiple physical quantities sensor based on nonreciprocal evanescent wave in the one-dimensional photonic crystals," *IEEE Sensors J.*, vol. 21, no. 18, pp. 19984–19992, Sep. 2021, doi: 10.1109/JSEN.2021.3100403.

[51] S. Chen, F. Fan, X. Wang, P. Wu, H. Zhang, and S. Chang, "Terahertz isolator based on nonreciprocal magneto-metasurface," *Opt. Exp.*, vol. 23, no. 2, p. 1015, Jan. 2015, doi: 10.1364/OE.23.001015.

[52] Y. Sharma, S. Prasad, and V. Singh, "Dispersion behavior of electromagnetic wave near the resonance in 1D magnetized ferrite photonic crystals," *Opt. Quantum Electron.*, vol. 50, no. 11, p. 410, Nov. 2018, doi: 10.1007/s11082-018-1677-8.

[53] B. T. Cunningham, M. Zhang, Y. Zhuo, L. Kwon, and C. Race, "Recent advances in biosensing with photonic crystal surfaces: A review," *IEEE Sensors J.*, vol. 16, no. 10, pp. 3349–3366, May 2016, doi: 10.1109/JSEN.2015.2429738.

[54] M. Herzberger and C. D. Salzberg, "Refractive indices of infrared optical materials and color correction of infrared lenses," *J. Opt. Soc. Amer.*, vol. 52, no. 4, p. 420, Apr. 1962, doi: 10.1364/JOSA.52.000420.

[55] E. D. Palik and G. Ghosh, *Handbook of Optical Constants of Solids*. San Diego, CA, USA: Academic, 1998.

[56] L. Qi, Z. Yang, F. Lan, X. Gao, and Z. Shi, "Properties of obliquely incident electromagnetic wave in one-dimensional magnetized plasma photonic crystals," *Phys. Plasmas*, vol. 17, no. 4, Apr. 2010, Art. no. 042501, doi: 10.1063/1.3360296.

[57] K. Artmann, "Berechnung der seitenversetzung des totalreflektierten strahles," *Annalen Physik*, vol. 437, nos. 1–2, pp. 87–102, Jan. 1948, doi: 10.1002/andp.19484370108.

[58] Z. A. Zaky, A. M. Ahmed, A. S. Shalaby, and A. H. Aly, "Refractive index gas sensor based on the Tamm state in a one-dimensional photonic crystal: Theoretical optimisation," *Sci. Rep.*, vol. 10, no. 1, Jun. 2020, Art. no. 9736, doi: 10.1038/s41598-020-66427-6.

[59] Y.-N. Zhang, T.-M. Zhou, B. Han, L. Zhang, and Q.-L. Wu, "Simultaneous measurement of hydrogen concentration and temperature based on fiber loop mirror combined with PCF," *IEEE Sensors J.*, vol. 18, no. 6, pp. 2369–2376, Mar. 2018, doi: 10.1109/JSEN.2018.2801831.

[60] Z. Huang et al., "Giant enhancement of the Goos–Hänchen shift based on quasi-bound states in the continuum in terahertz band through silicon based metasurface," *Opt. Commun.*, vol. 540, Aug. 2023, Art. no. 129507, doi: 10.1016/j.optcom.2023.129507.

[61] X. Jiang, B. Fang, and C. Zhan, "Theoretical enhancement of the Goos–Hänchen shift with a metasurface based on bound states in the continuum," *Micromachines*, vol. 14, no. 6, p. 1109, May 2023, doi: 10.3390/mi14061109.

[62] Y.-K. Shi, Y.-M. Liu, B.-F. Wan, and H.-F. Zhang, "A proposal of a laminated versatile sensor for refractive index and displacement with variable quality factor influenced by the graphene based on the reflected Goos–Hänchenn effect," *IEEE Sensors J.*, vol. 22, no. 18, pp. 17791–17798, Sep. 2022, doi: 10.1109/JSEN.2022.3196829.

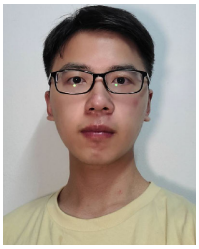

Yuan-Kun Shi was born in Jiangsu, China, in 2002. He is currently pursuing the bachelor's degree with the Nanjing University of Posts and Telecommunications, Nanjing, China, with a focus on investigating 1-D photonics crystals and Goos–Hänchen (GH) effect.

You-Ming Liu was born in Jiangsu, China, in 2002. He is currently pursuing the bachelor's degree with the Nanjing University of Posts and Telecommunications, Nanjing, China.

He engages in the research of zero-refraction materials.

Hai-Feng Zhang was born in Jiangxi, China, in 1978. He received the M.Sc. degree in electronics science and technology from Nanchang University, Nanchang, China, in 2008, and the Ph.D. degree from the College of Electronic and Information Engineering, Nanjing University of Aeronautics and Astronautics, Nanjing, China, in 2014.

He is currently working as a Professor with the College of Electronic and Optical Engineering and the College of Flexible Electronics (Future Technology), Nanjing University of Posts and Telecommunications, Nanjing. His main research interests include the computational electromagnetics, plasma photonic crystal, plasma stealthy, and electromagnetic properties of metamaterials and metastructures.